



HAL
open science

Single-pulse electrical stimulation methodology in freely moving rat

Eloïse Gronlier, Estelle Vendramini, Julien Volle, Agata Wozniak-Kwasniewska, Noelia Antón Santos, Véronique Coizet, Venceslas Duveau, Olivier David

► To cite this version:

Eloïse Gronlier, Estelle Vendramini, Julien Volle, Agata Wozniak-Kwasniewska, Noelia Antón Santos, et al.. Single-pulse electrical stimulation methodology in freely moving rat. *Journal of Neuroscience Methods*, 2021, 353, pp.109092. 10.1016/j.jneumeth.2021.109092 . hal-03553518

HAL Id: hal-03553518

<https://hal.science/hal-03553518v1>

Submitted on 10 Mar 2023

HAL is a multi-disciplinary open access archive for the deposit and dissemination of scientific research documents, whether they are published or not. The documents may come from teaching and research institutions in France or abroad, or from public or private research centers.

L'archive ouverte pluridisciplinaire **HAL**, est destinée au dépôt et à la diffusion de documents scientifiques de niveau recherche, publiés ou non, émanant des établissements d'enseignement et de recherche français ou étrangers, des laboratoires publics ou privés.



Distributed under a Creative Commons Attribution - NonCommercial 4.0 International License

1 **Title: Single-pulse electrical stimulation methodology in freely moving rat**

2

3 **Authors**

4

5 Eloïse Gronlier^{1-2*}, Estelle Vendramini², Julien Volle¹, Agata Wozniak-Kwasniewska¹,
6 Noelia Antón Santos², Véronique Coizet², Venceslas Duveau¹, Olivier David^{2,3}

7

8 ¹ : SynapCell SAS – Saint-Ismier, France – contact: egronlier@synapcell.fr

9 ² : Univ. Grenoble Alpes, Inserm, GIN, Grenoble Institut des Neurosciences, Grenoble,
10 France

11 ³ : Aix Marseille Univ, Inserm, INS, Institut de Neurosciences des Systèmes, Marseille,
12 France

13

14 * : corresponding author

15

16

17 **Abstract**

18

19 *Background:* Cortico-cortical evoked potentials (CCEP) are becoming popular to infer
20 brain connectivity and cortical excitability in implanted refractory epilepsy patients. Our
21 goal was to transfer this methodology to the freely moving rodent.

22 *New method:* CCEP were recorded on freely moving Sprague-Dawley rats, from cortical
23 and subcortical areas using depth electrodes. Electrical stimulation was applied using 1 ms
24 biphasic current pulse, cathodic first, at a frequency of 0.5 Hz, with intensities ranging
25 from 0.2 to 0.8 mA. Data were then processed in a similar fashion to human clinical
26 studies, which included epoch selection, artefact correction and smart averaging.

27 *Results:* For a large range of tested intensities, we recorded CCEPs with very good signal
28 to noise ratio and reproducibility between animals, without any behavioral modification.
29 The CCEP were composed of different components according to recorded and stimulated
30 sites, similarly to human recordings.

31 *Comparison with existing methods:* We minimally adapted a clinically-motivated
32 methodology to a freely moving rodent model to achieve high translational relevance of
33 future preclinical studies.

34 *Conclusions:* Our results indicate that the CCEP methodology can be applied to freely
35 moving rodents and transferred to preclinical research. This will be of interest to address
36 various neuroscientific questions, in physiological and pathological conditions.

37

38 **Keywords:** intracranial electroencephalography (iEEG), direct electrical stimulation
39 (DES), rodent, cortico-cortical evoked potentials (CCEP), local field potential (LFP)

40 1 Introduction

41 To investigate large neuronal networks, potentially impaired in psychiatric and
42 neurological conditions, an interesting approach is to use direct electrical stimulation
43 (DES), which is becoming popular in the field of epilepsy surgery. This method quantifies
44 the local field potential (LFP) responses to brief pulses of electrical current, so-called
45 single pulse electrical stimulation (SPES) (Keller et al., 2014; Matsumoto et al., 2004).
46 Those responses, or cortico-cortical evoked potentials (CCEP) when averaged over
47 stimulations, can be obtained using either depth electrodes
48 (stereoelectroencephalography, SEEG) or extra-cerebral electrodes
49 (electrocorticography, ECoG). We will only consider SEEG here.

50 DES combined with SEEG is a neurosurgical procedure commonly used to induce
51 seizures and to investigate brain connectivity in drug-resistant epileptic patients implanted
52 with intracranial electrodes (Borchers et al., 2012; David et al., 2010; David et al., 2013;
53 Young et al., 2018). Though the CCEP approach is promising to make significant
54 advances in our understanding of large-scale networks (Trebault et al., 2018), its use in
55 human is limited to patients with focal epilepsies, candidates to resective surgery, with
56 few possibilities to explore other configurations, in particular exploring the basal ganglia
57 (Enatsu et al., 2013; Kubota et al., 2013). CCEPs in human are composed of a quick and
58 early deflection (10-50 ms) which can be followed by a later slow component (50-250 ms)
59 (Keller et al., 2014; Matsumoto et al., 2004). The first component may correspond to a
60 local direct excitation whereas the second one may be linked with indirect mechanisms
61 and multisynaptic pathways (Entz et al., 2014; Eytan et al., 2003; Kubota et al., 2013;
62 Matsumoto et al., 2004). Peak latencies can vary among implanted structures, stimulation
63 parameters and recording techniques (Trebault et al., 2018). One of the most important
64 points for cortical stimulation is the choice of optimum stimulation parameters, such as
65 intensity, frequency and pulse width (Prime et al., 2018).

66 Electrical brain stimulation has been used for decades in freely-moving rodent models
67 under various conditions. For example, by applying paired-pulse stimuli in a rat model of
68 temporal lobe epilepsy, it was shown that LFP responses to stimulation were a good
69 approach to assess excitatory and inhibitory processes involved during epileptogenesis
70 (Queiroz et al., 2009). The paired-pulse stimulation paradigm has also been used in many
71 studies assessing neurotransmitter functions, including *in vivo* (e.g. (Cao and Stan Leung,
72 1992)). The SPES approach has been less used *in vivo*. In the 1980s, the group of
73 Klingberg studied cortical responses to subcortical stimulation. They recorded frontal
74 evoked potentials in freely moving rats after electrical stimulation of locus coeruleus and
75 showed the modulation of evoked responses under various pharmacological challenges
76 (Heller and Klingberg, 1989). They also studied somatosensory evoked responses after

77 stimulation of the trigeminal nuclei in freely moving rats and showed behavior-dependent
78 changes of evoked responses (Rehnig et al., 1987). Those behavior-dependent changes
79 were also reported in recorded responses in CA1 (Zosimovskii et al., 2008). In this study,
80 they stated that stimulation of Schaffer collaterals with single pulse current impulses could
81 evoke polysynaptic responses in hippocampal CA1 in freely moving rats. They also
82 observed delay variations in recorded responses of CA1 between awake and sleep states.
83 In another study, long-term synaptic depression and depotentiation were examined by
84 recording LFP evoked in sensorimotor cortex by stimulation of the white matter in freely
85 moving rats (Froc et al., 2000). They observed amplitude variations of evoked responses
86 after the delivery of a single low-frequency train (1Hz, 15min). More recently, Magill and
87 colleagues recorded in the subthalamic nucleus unit responses evoked by cortical
88 stimulation on anesthetized rats and showed that the shape of the subthalamic responses
89 was different according to the stimulated cortical area (Magill et al., 2004).

90 Despite the long history of electrical stimulation in experimental neuroscience, there is
91 finally very few preclinical reports using similar stimulation and recording protocols to the
92 ones used nowadays in epilepsy surgery for assessing functional connectivity using
93 SPES. We thus wanted here to translate the CCEP methodology for preclinical studies in
94 the freely moving rodent, by developing an experimental platform allowing to record
95 evoked responses to SPES in conditions very closed to those encountered in human
96 beings. Such a platform would help for drug development and find efficient ways for
97 screening new drugs in animal models *in vivo* before their application to clinical trials. The
98 present report summarizes the main steps to record successfully CCEPs in freely moving
99 rodent. To demonstrate the feasibility of this approach, we chose to study the connectivity
100 between the somatosensory cortex and the dorso-lateral part of the striatum because both
101 structures are directly connected. The corticostriatal pathway is known to integrate
102 information coming from the cortex (Pidoux et al., 2011). In addition to the direct
103 projections from the cortex toward the striatum, the latter has reciprocal feedback
104 projections going back to the cortex particularly through the subthalamic nucleus, globus
105 pallidus and thalamus (Alloway et al., 1998; Hintiryan et al., 2016). We should thus be
106 able to record both cortico-striatal and striato-cortical CCEPs. Those responses should
107 be similar to the ones observed in previous studies on anesthetized rats and humans, in
108 terms of CCEP definition with the possibility to clearly identify the two first components.

109 **2 Materials and methods**

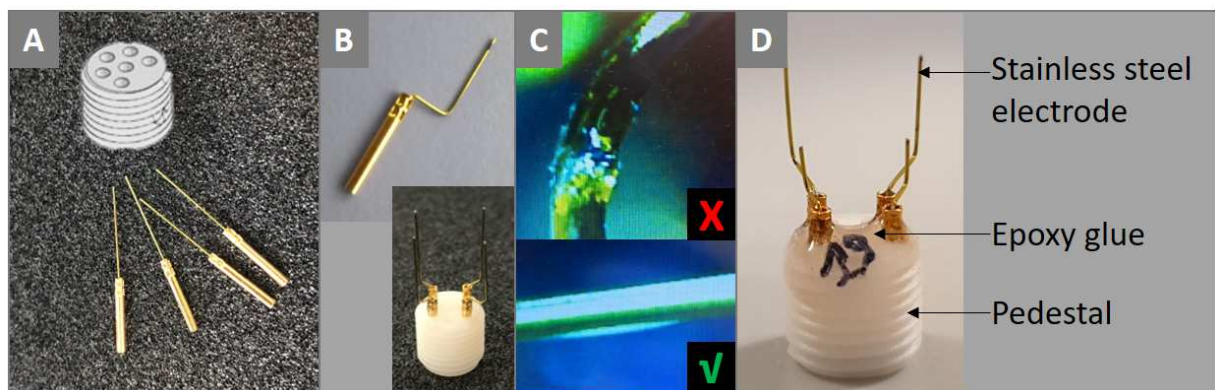
110 **2.1 Animals**

111 Twenty experimentally naive adult male Sprague-Dawley rats (Charles River) initially
112 weighing 170-200g were used. They were housed under a normal dark-light cycle (lights
113 off at 7pm), with constant dimmed light. Experimental procedures were performed during

114 the light phase of the daily cycle. Animals had free access to food and water, except during
115 recording sessions and when their weight became higher than a threshold of 400g, they
116 were put under dietary restriction (only 15g a day of dry food). They were maintained
117 following the guidelines set for the care and use of laboratory animals by the European
118 Union (directive 2010/63/EU), with controlled temperature and humidity conditions. The
119 protocol used to complete this study was reviewed and approved by the Ethical Committee
120 of Grenoble Institute of Neurosciences (University Grenoble Alpes).

121 2.2 Electrode configuration

122 Electrode configuration is important to be considered to achieve appropriate current
123 distribution between the anode and cathode, while recording brain responses with good
124 signal to noise ratio. Inappropriate geometry and cabling can generate local current
125 density inhomogeneities, which can lead to either poor neuronal responses or to tissue
126 damages (Campbell and Wu, 2018; Merrill et al., 2005). In practice, to speed up the
127 process of electrode implantation while maximizing the reproducibility of electrode
128 positioning, electrodes were prepared before surgery on a pedestal. We used four
129 stainless steel polyimide-coated electrodes (0.2 mm diameter, 10 mm length, stranded,
130 Plastics One, E363/2/SPC) and one pedestal (Plastics One, MS363) per animal (see
131 Figure 1.A). Then we bent and cut electrodes at specific length to target the desired brain
132 areas (see Figure 1.B). At this step, it is important to check the coating integrity with a
133 microscope (e.g. see Figure 1.C with a damaged coating at the top and a preserved one
134 at the bottom). Electrodes with damaged coating were replaced. Finally, electrodes were
135 glued to the pedestal using dental cement (see Figure 1.D). Electrode impedances were
136 measured to verify balanced values across all electrode sites. Because of space
137 constraints, we were limited to a number of 6 electrodes, including two electrodes for the
138 reference and ground.



139
140
141
142
Figure 1: Electrodes' setup manufacturing. A. Take a pedestal and electrodes (four stainless steel depth electrodes here). B. Bend them and cut them at the desired lengths and angles to target brain areas you want. C. Check under a microscope the coating integrity. D. Finally, glue all electrodes to the pedestal.

143 **2.3 Surgical procedure**

144 Animals were allowed to acclimate to the facility for at least one week after their arrival.
145 Then, they were implanted using aseptic surgical procedures. Animals were first
146 anesthetized with isoflurane (2.5% induction, 2.5% maintain, 0.5 L/min O₂) with body
147 temperature maintained at 36°C. They received topical buprenorphine subcutaneously
148 just before the surgery for reducing pain (0.05 mg/kg). The head was shaved, and the rat
149 placed in a stereotaxic apparatus. Then the scalp was swabbed with betadine and a
150 central incision was made to expose the skull. Small holes were drilled in the skull at the
151 desired coordinates, and four electrodes were lowered bilaterally into the somatosensory
152 cortex and the striatum. For the somatosensory cortex, the coordinates used were: -2.92
153 mm antero-posterior, ±3 mm medio-lateral and -1.2 mm dorso-ventral, relative to bregma.
154 For the striatum, the coordinates used were: +0.24 mm antero-posterior, ±3.6 mm medio-
155 lateral and -4.6 mm dorso-ventral, relative to bregma. Two skull screws were also added:
156 one over the prefrontal cortex (used as ground and reference electrode) and one over the
157 cerebellum (E363/96/1.6/SPC, Plastics One). The recording headstage was then secured
158 to the cranium with dental acrylic using two skull screws as anchors. Finally, animals were
159 housed individually and given at least one week to recover after surgery before beginning
160 any experimental procedures. During this period, the habituation process took place to
161 allow animals to become familiar with the recording environment.

162 At the end of experiments, animals were sacrificed, and brains collected for histological
163 evaluation. Animals were deeply anesthetized with isoflurane and an injection of
164 pentobarbital (Exagon, 1.5 mL/kg i.p.) was made. Under deep anesthesia, electrolytic
165 lesions were made: a 60 s anodic monophasic current of 100 µA was passed through all
166 electrodes. The animals were then terminally perfused transcardially with a 0.9% saline
167 solution. The brains were removed and stored at -80°C before sectioning. 40-micrometer
168 coronal sections were collected with a cryostat and mounted on slides, stained with Nissl
169 coloration and coverslipped. Analyses were conducted using a microscope (Nikon Eclipse
170 80i) to verify electrodes placement.

171 **2.4 Recording and stimulation protocols**

172 A protocol reproducing clinical routine conditions was designed to stimulate and record
173 from all possible anatomical configurations. Stimulation parameters were chosen based
174 on bibliographic analysis and previous experiments to induce asymptomatic
175 electrophysiological responses only. The objective here was to record high quality signals
176 with good reproducibility across animals to be able to compare evoked responses
177 between them.

178 Before undergoing any experimental manipulation, each animal was subjected to several
179 acclimation sessions where the subject was tethered to the recording system and allowed
180 to move freely in the recording chamber, which consisted of a Plexiglas chamber placed
181 within a sound-attenuating box. This shielded room (Faraday box) allowed to limit line
182 noise and any other external signal contamination. Electrical stimuli were generated with
183 an isolated stimulator (DLS100, World Precise Instruments, Sarasota, USA) triggered by
184 a DS8000 unit (World Precise Instruments, Sarasota, USA). All data were recorded using
185 a Micromed acquisition system (SD LTM 6400 Express EEG 64 channels, Treviso, Italy)
186 in which they were amplified, filtered and digitized (sampling rate: 1024 Hz, band-pass
187 filter: 0.008 – 150 Hz, 22-bit analog to digital converters). A unipolar (referential) montage
188 was used against a common reference placed on the prefrontal screw, which also served
189 as ground.

190 Stimulation pattern was set to a 1 ms biphasic square pulse composed of a negative
191 phase followed by a positive one (pulse width of 0.5 ms/phase). Maximal pulse intensity
192 was set to 0.8 mA, which corresponds to a maximal charge per phase of 0.4 μC and a
193 maximal charge density of 1274 $\mu\text{C}/\text{cm}^2/\text{phase}$ given the electrode section. These
194 maximum figures were under values used in previous studies on patients (David et al.,
195 2013) and rats (Magill et al., 2004), with 1800 $\mu\text{C}/\text{cm}^2/\text{phase}$ and 2293 $\mu\text{C}/\text{cm}^2/\text{phase}$
196 respectively. Another important parameter is the frequency of stimulation. We chose to
197 apply a 0.5 Hz stimulation to reduce the probability of inducing any potentiation while being
198 able to record single responses at a fast rate. This inter-stimulus interval of 2 seconds
199 also allowed the signal to return to baseline between two stimulations.

200 The stimulation protocol spanned sequentially all electrodes, while recording on all other
201 electrodes. The minus electrical connector was alternatively connected to the
202 somatosensory cortex or to the striatum of one hemispheric side. The screw over the
203 cerebellum was used as the positive terminal of the stimulation. Each animal underwent
204 the following stimulation protocol:

- 205 ▪ 15 minutes of acclimation to wait for calm and stability
- 206 ▪ 3 minutes of baseline while recording without any stimulation
- 207 ▪ Different intensities of stimulation applied during 2 minutes at 0.5 Hz (60
208 stimulations in each train) starting from 200 μA up to 800 μA , by steps of 200 μA .

209 All animals underwent this stimulation protocol for each of its four structures (striatum right
210 and left, somatosensory cortex right and left), in a randomized order. During the recording
211 session, the vigilance level was controlled by maintaining the animal awake.

212 **2.5 Data analysis**

213 Signals were analyzed offline with scripts written in Matlab (2018, version 9.4.0 R2018a,
214 Natick, Massachusetts: The MathWorks Inc.). Most part of Matlab scripts came from the
215 open-source ImaGIN toolbox (<https://f-tract.eu/software/imagin/>). One script have been
216 specifically developed based on the exponential fit developed in (Conde et al., 2019).

217 **2.5.1 Stimulation detection and epoching**

218 Electrical stimulation induces the presence of stimulation artefacts lasting few
219 milliseconds and composed of a sharp deflection (Trebaul et al., 2016). We used this
220 sharp deflection to detect automatically the time of each stimulation (David et al., 2013).
221 Then, signals were cropped around each stimulation (epoching): 400 ms pre-stimulus and
222 1100 ms post-stimulus, relative to time origin on the beginning of the stimulation artefact.

223 **2.5.2 Artefact correction**

224 Each epoch was baseline-corrected from -400 to -3 ms. In each of these epochs,
225 stimulation artefacts were removed by interpolating the interval between -3 ms and +6 ms
226 using an autoregressive model (*fillgaps.m* Matlab function). The polarization of the
227 electrodes by the stimulation may result in a decay artefact affecting up to hundreds of
228 milliseconds of signal. To correct this decay, we subtracted from each epoch the best fit
229 of a decreasing two-exponential decay function as used in (Conde et al., 2019). To do so,
230 we used a parameterized model of the artefact: $Ae^{-Bt} + Ce^{-Dt} + E$, where time t was chosen
231 starting at the end of interpolation (+6 ms) and ending between 50 and 400 ms post-
232 stimulation (step of 50 ms). For each time window, the parameters were optimized using
233 nonlinear regression (*nlinfilt.m* Matlab function) and we computed the goodness of fit
234 defined as the sum of the square of the difference between the original signal and the
235 fitted values, normalized by the sum of the squared signal. Then, we selected the time-
236 window for which this indicator was maximum and subtracted the corresponding fitted
237 model artefact from raw data.

238 **2.5.3 Trial selection**

239 Bad trials were automatically detected and removed from further analyses with an analysis
240 which excluded trials showing a response energy 3 times higher than the median
241 response energy over the whole stimulation run (David et al., 2013). A semi-automated
242 motion artefact detector was developed to remove visually contaminated signal periods
243 which were mainly due to transient high motor activity of the animal. It pre-selected values
244 higher than 95% of the maximum of the z-scored signal envelop. Finally, exclusion was
245 validated or not by visual inspection.

246 **2.5.4 Average and DC offset correction**

247 Responses were averaged together over trials and obtained CCEPs were baseline-
248 corrected according to the [-400 -3] ms pre-stimulus time period.

249 **2.5.5 Signal quality and intensity selection**

250 Signal quality was assessed by computing the signal-to-noise ratio (SNR) of the evoked
251 responses obtained for each stimulation intensity used. For each CCEP of each intensity
252 of stimulation, the SNR was defined by dividing the power of the signal during the evoked
253 response (between 0 and 150 ms) by the power of the signal during baseline (between -
254 400 and -50 ms). Then, an arbitrary threshold on SNR (10 dB) was used to consider
255 CCEPs of sufficient amplitude. To complement this indicator of signal quality, we
256 computed the correlation index between each individual trial and the averaged CCEP, for
257 each intensity of stimulation. We also assessed signal stability by computing the
258 correlation of the averaged signal on the 15 first stimulations to the 15 last ones.

259 **2.5.6 Time-frequency decomposition and statistics**

260 Time-frequency decomposition of CCEPs was performed using a Multitaper method
261 (Hanning window) with *ft_specest_mtmconvol* function of FieldTrip (Oostenveld et al.,
262 2011). The sliding temporal window length was chosen as 100 ms and time resolution of
263 10 ms (1 Hz spectral resolution). This window spans first early components of the evoked
264 response, rendering it impossible to characterize frequency content over the first 10 ms.
265 However, any further reduction of this window length would lead to an undesirably poor
266 frequency resolution. Afterwards, time-frequency maps were normalized (Z-score) on pre-
267 stimulation period between -400 and -50 ms.

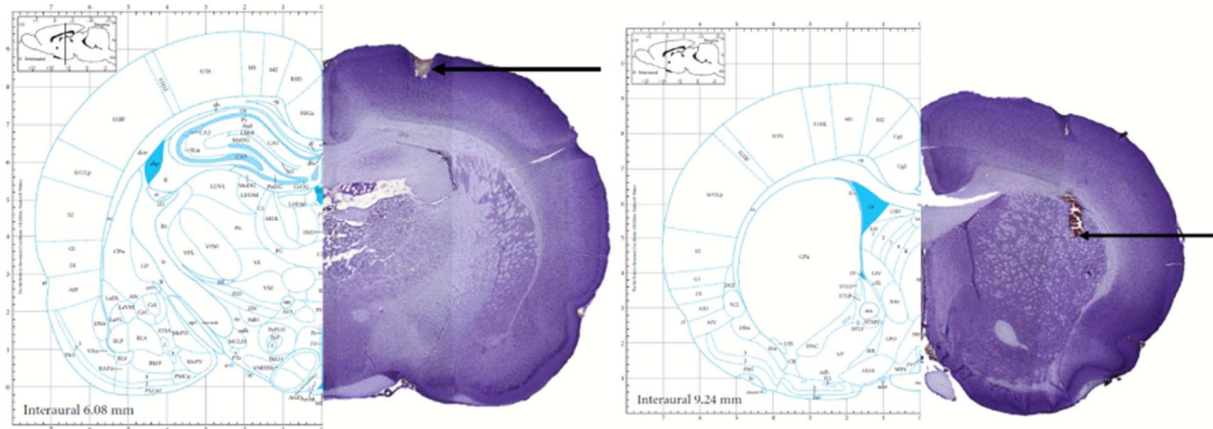
268 The specific spectral signature of CCEP for each stimulated structure was identified at the
269 group level using a dedicated statistical analysis, which implemented a random-effect
270 group analysis in the framework of Statistical Parametric Mapping 12 (SPM) software
271 (www.ion.ucl.ac.uk/spm12). This two-level hierarchical model was previously described in
272 (Kiebel and Friston, 2004). Data normality was verified using Shapiro-Wilk test. The first
273 level (intra-individual) statistical analysis performed for each animal was a one-sample t-
274 test across time-frequency maps of each trial at a given intensity of stimulation. This first
275 level analysis was used to provide appropriate summary statistics (effect size, or beta
276 maps in SPM terminology) at the individual level and for each structure, which were then
277 used as input for the second-level analysis assessing across animals' effects (group
278 analysis). This second step implemented a one-sample t-test to identify the reproducible
279 response for each region, and a two-sample t-test to identify differences between regions.

280 **2.5.7 Statistical analyses**

281 Descriptive statistics were used for studying signal stability using correlation index. Across
282 stimulation intensities' comparisons (on correlation and powers) were assessed using
283 non-parametric Wilcoxon signed rank tests due to non-normal data distribution. Those
284 statistical analyses were performed using GraphPad Prism software (version 9.0.0 for
285 Windows, GraphPad Software, San Diego, California USA, www.graphpad.com) with a
286 significance level of $\alpha=0.05$.

287 3 Results

288 From the results of histological analyses (see Figure 2), only three electrodes amongst all
289 recordings were discarded due to their position outside the anatomical target. One animal
290 lost its pedestal during housing and was recorded for only one site of stimulation.
291 Electrodes impedance measurements were around 30 k Ω on average (min: 20 k Ω ; max:
292 100 k Ω).



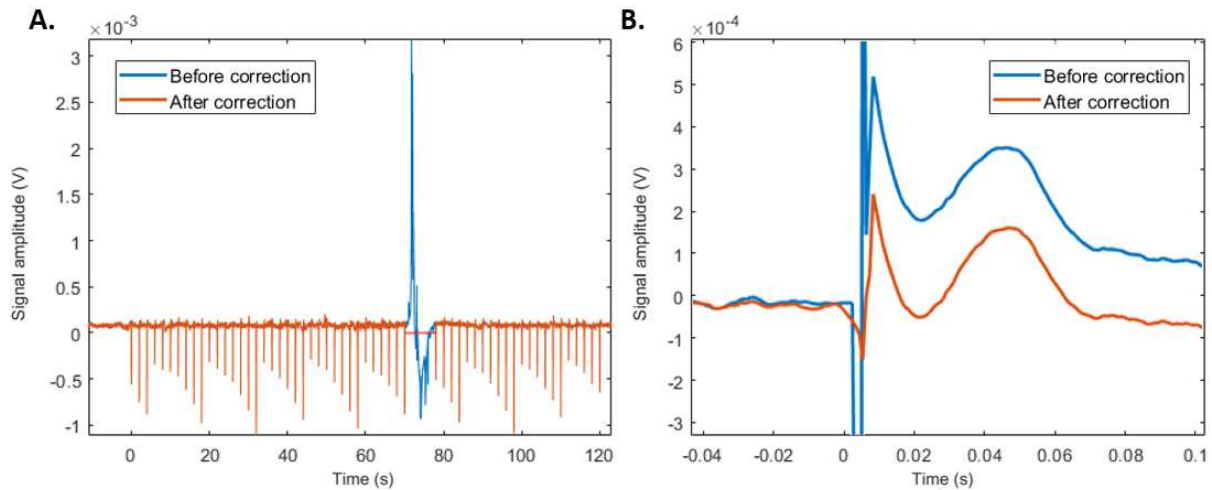
293
294 *Figure 2: Histological pictures after electrolytic lesion and Nissl staining for validate electrodes localizations (in the*
295 *somatosensory cortex on the left and in the dorso-lateral striatum on the right).*

296 3.1 Methodology validation

297 Figure 3A shows an example of the output of the semi-automated detection of periods
298 with large movement artefacts or line noise. The principle of the preprocessing approach
299 for automated data selection was to discard such data from the downstream processing
300 of CCEPs. On average, 64 trials were kept for further analyses for striatum stimulation
301 and 66 trials for somatosensory stimulation (min. 61 / max. 71 for striatum, min. 58 / max.
302 94 for somatosensory cortex) for each amplitude of stimulation. This corresponded to 79%
303 of recorded data.

304 The artefact correction method was globally efficient to remove the low frequency drift of
305 the amplifier that could occur after the stimulation. It also allowed to remove the initial

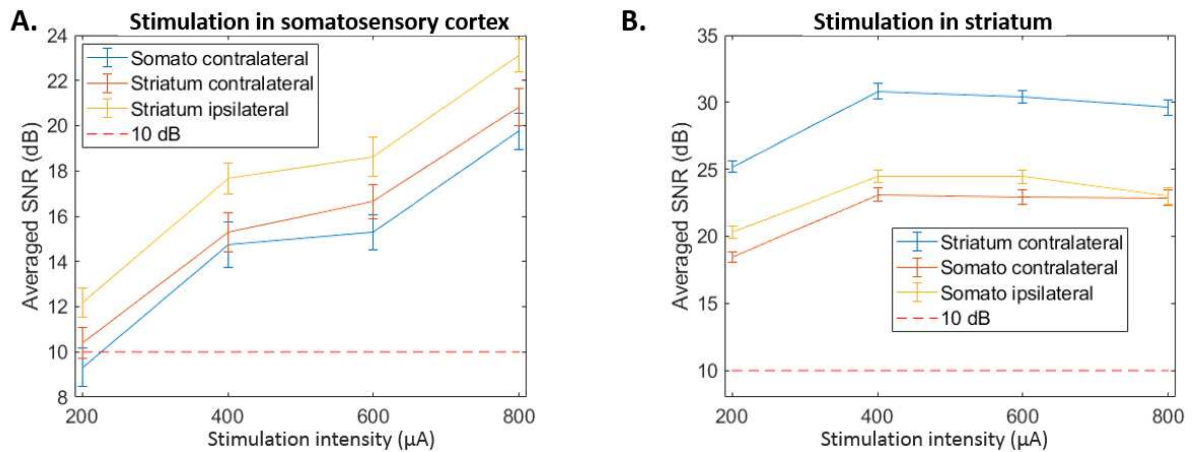
306 sharp deflection, but without recovering the neuronal signal during the interpolation period,
307 set to [-3; 6] ms (example of artefact correction shown in Figure 3B).



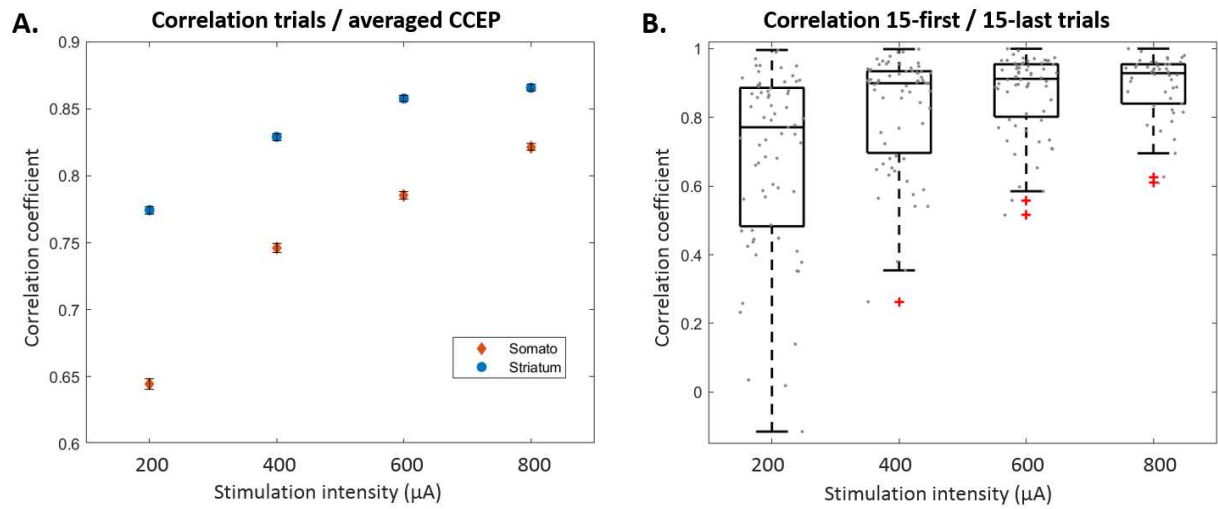
308
309 *Figure 3: A. Example of semi-automated movement artefact period removal. The blue excluded part of the signal*
310 *seems to be due to brief movement of the animal. B. Example of artefact correction using a short interpolation*
311 *combined with a longer exponential fit (blue before correction and red after). This correction allows to free from the*
312 *return-to-zero time of the system and the sharp deflection of the stimulation artefact.*

313 Then, we selected the optimum intensity of stimulation for each animal. To do so, we
314 plotted dose-response curves corresponding to the signal to noise ratio (SNR) of the
315 amplitude of the evoked response compared to baseline, as a function of the intensity of
316 stimulation. For example, Figure 4 shows the averaged dose-response curve, across
317 animals, of the response after stimulation in the somatosensory cortex (A) and in the
318 striatum (B). The SNR was rapidly above the selected threshold of 10 dB except for some
319 animals at the lowest intensity of 200 μ A. When the striatum was stimulated, increasing
320 intensity above 400 μ A did not increase the averaged SNR which reached a plateau. We
321 also computed, for each intensity of stimulation and each structure, the correlation
322 coefficient between each trial and the CCEP obtained by averaging all trials, which is a
323 good measure of the SNR at the single-trial level (see Figure 5). We obtained increasing
324 correlation coefficients with the intensity going from 64% up to 82% for the somatosensory
325 stimulation and from 77% up to 87% for the striatal one, with higher values for the striatum
326 than for the somatosensory cortex (Figure 5.A). To assess for changes in the response
327 shape, we computed the averaged CCEP over the first and last fifteen stimulations,
328 separately, and computed their cross-correlation as a measure of reproducibility. We
329 found good stability of signals at 400 μ A stimulation compared to lower intensity with a
330 median correlation index of 90% versus 77% at 200 μ A (Figure 5.B). At higher intensities,
331 the correlation index (CI) is significantly higher compared to 400 μ A (Wilcoxon test: 200 μ A
332 vs. 400 μ A, 400 μ A vs. 600 μ A and 600 μ A vs. 800 μ A: $CI_{\text{median } 200\mu\text{A}}=0.77 < CI_{\text{median } 400\mu\text{A}}=0.90$

333 $< CI_{\text{median } 600\mu\text{A}}=0.91 < CI_{\text{median } 800\mu\text{A}}=0.93$, $p\text{-value}<0.001$, $N=213$). As observed here, the
 334 SNR of the evoked response and correlation index increase with stimulation intensity but
 335 we had to fix a limit to avoid any behavioral effect. So we had a compromise between
 336 selecting the lowest intensity producing good evoked responses while not inducing any
 337 undesirable effect. From these tuning curves, we selected 400 μA intensity for further
 338 experiments, as we evaluated the corresponding SNR of sufficient amplitude and already
 339 good correlation index values. We also verified power stability between the beginning of
 340 the recording (15-first stimulations) and the end (15-last) (using *bandpower.m* in Matlab)
 341 but we obtained no significant difference (results not depicted here, Wilcoxon test, $N=69$,
 342 $p=0.14$ at 200 μA , $p=0.26$ at 400 μA , $p=0.29$ at 600 μA and $p=0.30$ at 800 μA). These
 343 analyses suggested little potentiation induced by repeated stimulations.



344
 345 *Figure 4: Averaged signal to noise ratio curves for somatosensory cortex stimulation (on the left, $N_{\text{min}} = 37 / N_{\text{max}} =$*
 346 *39 recordings) and for the striatum (on the right, $N_{\text{min}} = 37 / N_{\text{max}} = 40$ recordings) for each intensity of stimulation*
 347 *(error bars are standard error of the mean values).*



348
 349 *Figure 5: On the left (A), averaged correlation coefficient between individual trials and CCEP for each intensity of*
 350 *stimulation (for stimulation in the somatosensory cortex in red and in striatum in blue, with SEM superimposed) (N_{min}*
 351 *= 2822 / N_{max} = 3247 trials). On the right (B), boxplot of correlation coefficients between 15-first and 15-last evoked*
 352 *responses for each intensity of stimulation for all animals and all electrodes (N = 213 electrodes, with individual values*
 353 *superimposed).*

354 **3.2 Temporal and spectral analysis of CCEP**

355 SPES of the striatum and the somatosensory cortex generated robust CCEPs quantifiable
 356 at the single-trial level, which were observed at both local (in contralateral structure) and
 357 remote cortical regions (in somatosensory cortex and striatum respectively). The inter-
 358 animal variability of recorded evoked responses was very low, as indicated by small
 359 values of the standard error of the mean (SEM) (see Figure 6). The shape of CCEP was
 360 also preserved between left and right hemispheres.

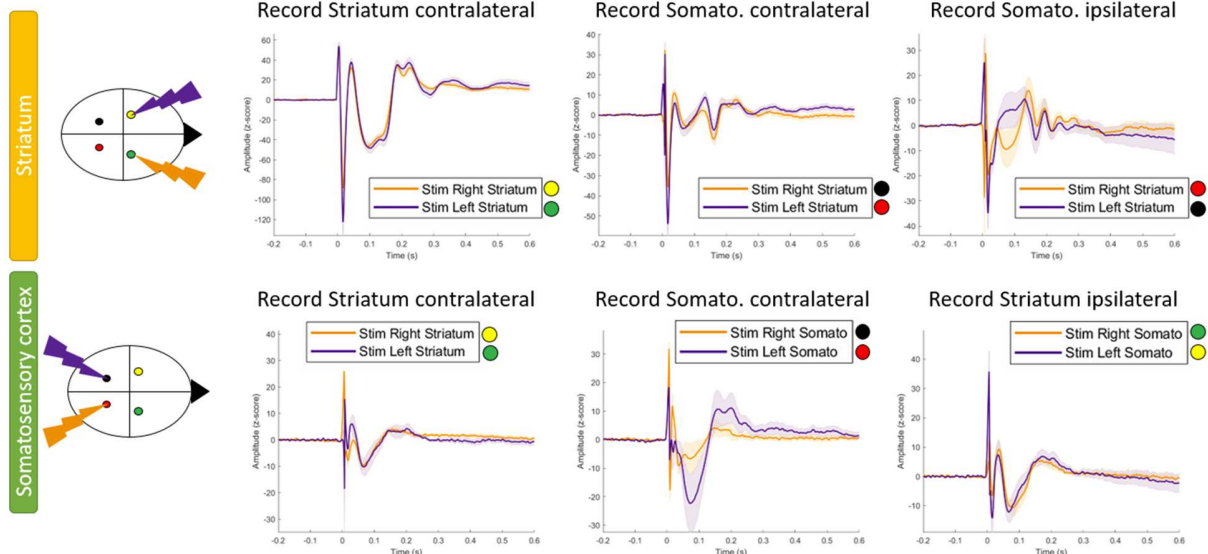
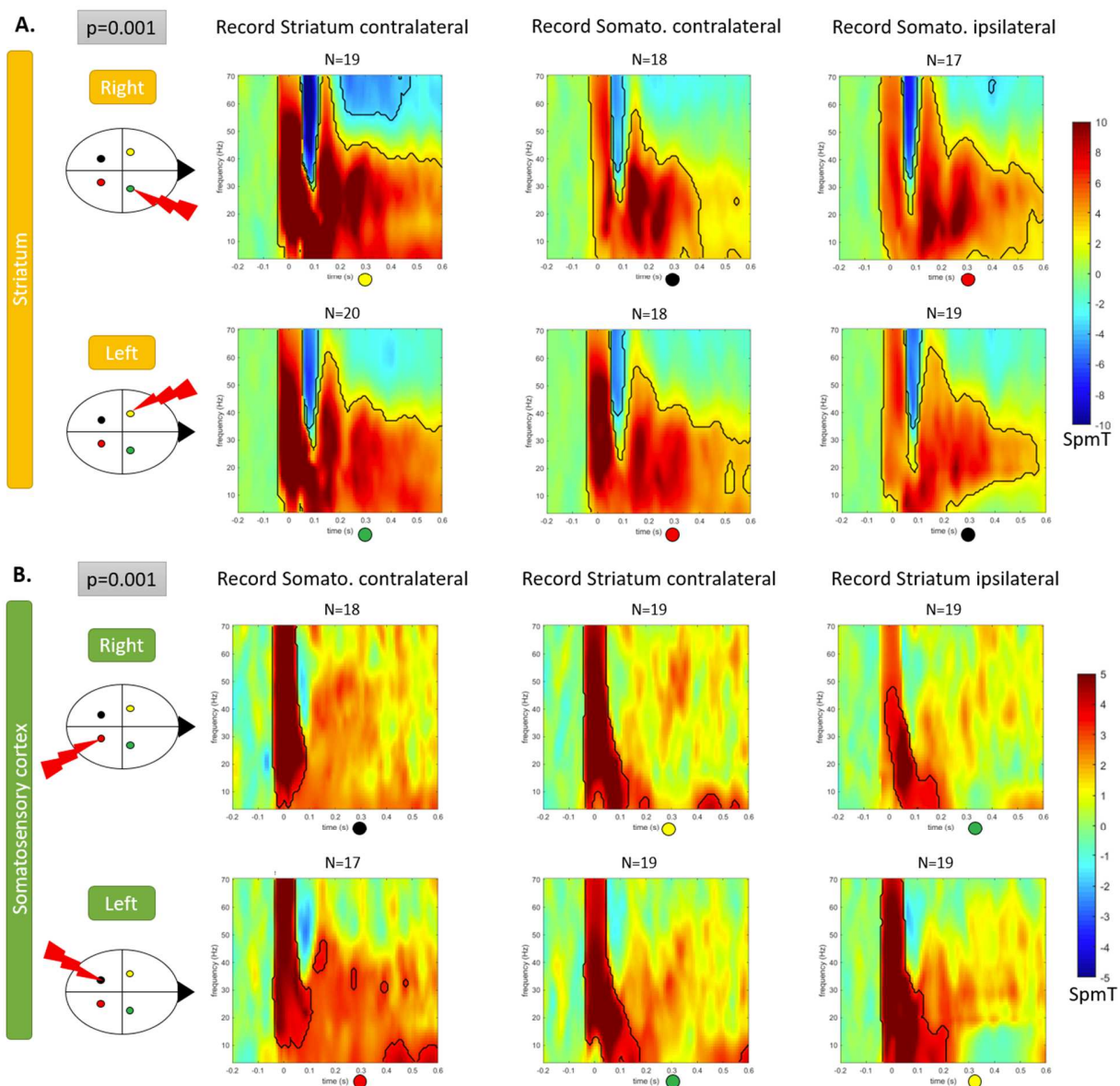


Figure 6: Averaged evoked responses ($N_{min} = 17$ and $N_{max} = 20$ animals) and standard errors of the mean (SEM) for each stimulated structure (striatum at the top and somatosensory cortex at the bottom) and each recorded electrode.

361
362
363
364

365 CCEPs obtained after a stimulation in the striatum showed more complex temporal
366 signatures, with longer oscillations up to 500 ms post-stimulation, than CCEPs obtained
367 after a stimulation in the somatosensory cortex for which the responses ended at
368 maximum 300 ms (Figure 6). Figure 6 also shows that stimulation in the striatum induced
369 responses of higher amplitudes than a stimulation in the somatosensory cortex. Those
370 differences are very well brought out by time-frequency analysis (Figure 7), with clearly
371 longer responses after a stimulation in the striatum than in the somatosensory cortex. On
372 this figure, surrounded area means a significance level of $p \leq 0.001$.



373

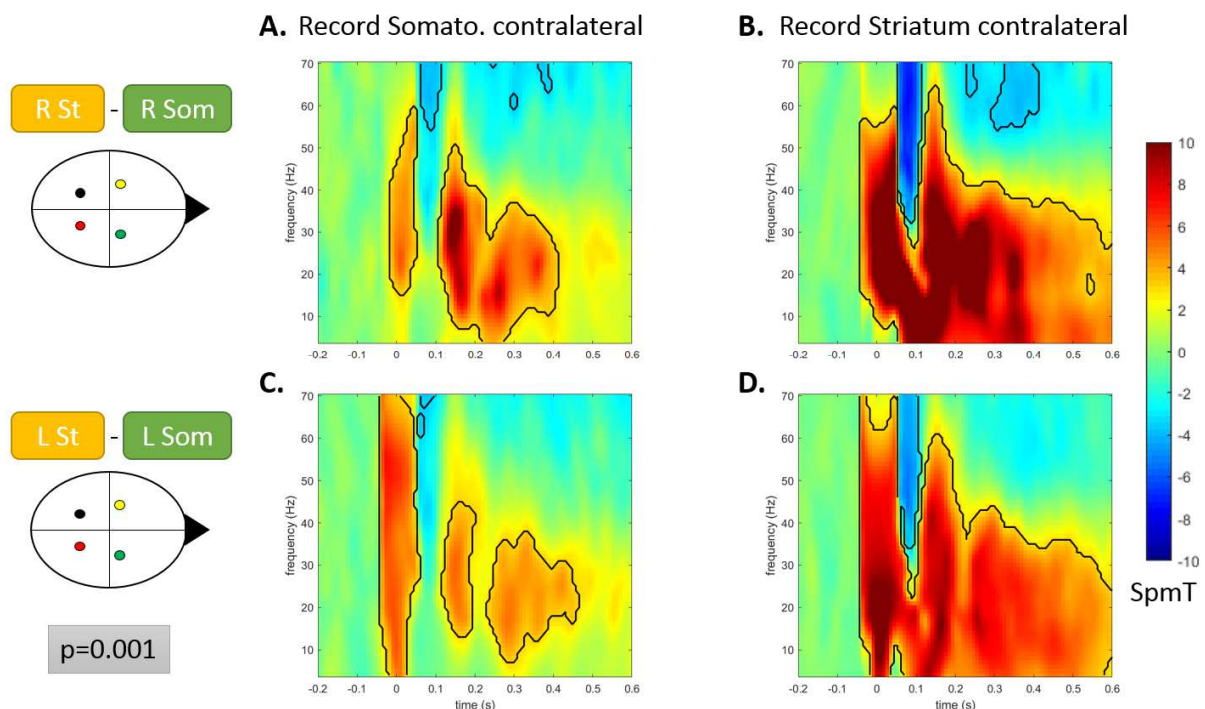
374
375
376
377
378
379
380
381

Figure 7: Statistical analysis on time-frequency maps resulting from a first step of statistic intra-animals consisting in a one-sample t-test across 2s-epochs of time-frequency maps of each animal at the selected intensity of stimulation (number of 2s-epochs taken into account: between 19 and 64 for the striatal stimulation and between 35 and 84 for the somatosensory cortex stimulation, data normality verified with Shapiro-Wilk test). Followed by a second step which is a two-sample t-test inter-animals allowing to identify the specific pattern of response obtained for each structure stimulated, for stimulation in striatum (A) and in somatosensory cortex (B). Surrounded areas are for a significance level of $p < 0.001$. Group sizes are noted above each statistical map ranging from 17 to 20 animals.

382
383
384

When comparing striatal and somatosensory responses, we obtained statistical maps that highlighted significant differences in the spectral content of CCEPs. Figure 8 shows the statistical results of the differences in the evoked responses between striatal and

385 somatosensory stimulation with significant values surrounded by a black line ($p \leq 0.001$).
 386 For example, Figure 8A shows the statistical difference between the evoked response
 387 recorded in the left somatosensory cortex after stimulation in the right striatum compared
 388 to the evoked response recorded in the same structure but after stimulation in the right
 389 somatosensory cortex. Other panels show different stimulation-recording configurations.
 390 First, one can identify that responses are of higher amplitudes after striatal stimulation
 391 compared to somatosensory one, as the t-maps are dominated by positive (red) values.
 392 Second, one can clearly see the presence of later components in striatal responses
 393 (Figure 8B and 8D), that are less present in somatosensory responses (Figure 8A and
 394 8C).



395
 396 *Figure 8: Statistical comparison of evoked responses between somatosensory stimulation and striatum stimulation. A*
 397 *and B for stimulations in right hemisphere, and C and D in the left one. A and C are recorded in the contralateral*
 398 *somatosensory cortex, and B and D in the contralateral striatum. Surrounded areas are significant values with*
 399 *$p \leq 0.001$ (two-sample t-test, $N_{min} = 17 / N_{max} = 20$ animals).*

400 To sum up, the two sites of stimulation (somatosensory cortex or striatum) produced highly
 401 significant, reproducible and regionally-specific CCEP.

402 4 Discussion

403 We have demonstrated that the CCEP methodology can be adapted for preclinical studies
 404 in freely moving animals. Strikingly, we observed reproducible recordings between
 405 animals, and response features that significantly differ between brain regions, which

406 suggests a high potential for this approach to provide important new types of information
407 in various animal models and experimental conditions in future studies. Below, we discuss
408 the most important issues for a successful implementation of the methodology.

409 **4.1 Stimulation parameters**

410 We used a limited number of electrodes in this proof-of-concept study: only 6, including
411 reference and ground electrodes, meaning 4 electrodes available for stimulation and
412 recording. This is not sufficient for describing large network properties across brain
413 regions, which would require significant improvements of surgical procedures. However,
414 the CCEP methodology *per se* does not depend on the number of implanted electrodes
415 and one can expect to have similar results with more electrodes, but with better spatial
416 resolution. Using smaller electrodes though would require to recalibrate stimulation
417 parameters as the section of electrodes is an important parameter because it influences
418 directly the current density for a given applied current.

419 **4.2 Electrode material**

420 Even if most clinical studies use platinum based electrodes (Cogan, 2008; Merrill et al.,
421 2005), stainless-steel polyimide coated electrodes meet several of the requirements of
422 the optimal device reviewed by Merrill and colleagues (Merrill et al., 2005). In addition to
423 their lower price, stainless-steel electrodes were shown to evoke less tissue response
424 than platinum (Dymond et al., 1970; Geddes and Roeder, 2003; Robinson and Johnson,
425 1961). Stainless steel and polyimide are biocompatible materials which are not toxic for
426 surrounding tissues (Babb and Kupfer, 1984; Stieglitz and Meyer, 1999). Moreover, the
427 mechanical strength of this material is high enough to go through the meninges and keep
428 its integrity for all the duration of experiments. Meantime it is also flexible enough to follow
429 small movements between tissues and the device (Rousche et al., 2001). Because we
430 used constant current stimulation and single pulses of large duration, we predict little
431 change to our main results in case of change of electrode material as the capacitive effect
432 of tissue electrode interface, which acts as a low pass filter, is minimal in SPES stimulation
433 compared to high frequency stimulation. The geometry of the electrode is however
434 important as it directly sets the charge density in current stimulation, which is a critical
435 factor achieving neuronal excitability.

436 **4.3 Data interpretation**

437 This methodology allows to record stable evoked responses across time (Figure 6) and
438 across subjects (Figure 7). To our knowledge, such inter-individual reproducibility is not
439 easily demonstrated in human's studies, where CCEP morphology can vary across
440 patients (Enatsu et al., 2013; Kubota et al., 2013). CCEP waveform heterogeneity is also
441 encountered at the individual scale across recording sites (Keller et al., 2014) and its

442 variability may be highly dependent on patient's state (Kunieda et al., 2015). Cortical
443 evoked responses after deep structures stimulation have been recorded in previous
444 studies such as in the thalamus of patients with drug-resistant epilepsy (Rosenberg et al.,
445 2009) or in the STN of Parkinsonian patients (Hartmann et al., 2018). To our knowledge,
446 it is however the first time that cortico-striatal and striato-cortical CCEP are documented.
447 Our results suggest the consideration of components significantly later than the classical
448 N1/N2 waves used in the standard CCEP taxonomy (Kunieda et al., 2015; Matsumoto et
449 al., 2004). The historical definition based on one early component N1 (around 10-30 ms)
450 and one late component N2 (around 80-250 ms) indeed does not encompass the
451 components we have observed up to 500 ms. Interestingly, a previous study using
452 subthalamic nucleus deep brain stimulation in rats also observed those late components
453 and showed that they had different biophysical origins (Kumaravelu et al., 2018). They
454 showed that long-latency responses were coming from polysynaptic activation of layer 2/3
455 pyramidal neurons via the cortico-thalamic-cortical pathway (Kumaravelu et al., 2018).
456 These indirect mechanisms involving multisynaptic pathways of the cortico-subcortico-
457 cortical loop have also been reported in clinical data (Eytan et al., 2003; Kubota et al.,
458 2013). This functional connectivity implies the cortico-subcortico-cortical pathway from
459 which several neural groups participate in feed-forward (cortico-subcortical) and feed-
460 back (subcortico-cortical) projections between those structures. One possible cause of
461 longer responses to the striatal stimulation is that more neuronal populations of the retro-
462 control loop going from the striatum toward the cortex are stimulated and activated.
463 Further investigations are needed to identify specifically the components of these
464 networks.

465 **5 Conclusion**

466 We presented here a new methodological process for recording LFP simultaneously to
467 electrical intracerebral stimulations in rodents. With this setup, we recorded high quality
468 signals, demonstrating that this approach is potentially relevant for future preclinical
469 studies. Such recordings would indeed open the opportunity to infer brain connectivity in
470 various deep brain structures impossible to explore with concomitant cortical sampling in
471 patients. Furthermore, combining this methodology with pathological animal models
472 should enable the identification of impaired brain networks and/or mechanisms of action
473 of novel drug compounds.

474

475 **Acknowledgements**

476 Authors gratefully acknowledge the support of European Research Council (ERC-2017-
477 PoC, Grant ID 790093, “EXCITATOR: Active probing of brain excitability by electrical
478 micro-stimulations for drug discovery”). This work was funded by Région Auvergne-
479 Rhône-Alpes under the grant agreement 2017 FRI Transfert EXCILAB. The study was
480 also supported by “Association Nationale Recherche Technologie” (ANRT, CIFRE
481 n°2017/1269, France).

482

483 **CRedit authorship contribution statement**

484 **Eloïse Gronlier:** conceptualization, methodology, software, formal analysis,
485 investigation, data curation, writing – original draft, visualization; **Estelle Vendramini:**
486 investigation, formal analysis ; **Julien Volle:** conceptualization, methodology, resources ;
487 **Agata Wozniak-Kwasniewska:** software, formal analysis; **Véronique Coizet:** resources;
488 **Noelia Antón Santos:** software, investigation; **Venceslas Duveau:** conceptualization,
489 methodology, validation, resources, writing – review and editing, supervision, project
490 administration, funding acquisition; **Olivier David:** conceptualization, methodology,
491 software, validation, formal analysis, resources, writing – review and editing, supervision,
492 project administration, funding acquisition

493

494 **Data accessibility**

495 The datasets generated during and/or analyzed during the current study, or support with
496 the code are available from the corresponding author on reasonable request.

497

498 **Declarations of interest**

499 EG, JV, AW and VD are employees of SynapCell. There is no other potential
500 conflict of interest to be disclosed.

501 **References**

- 502 - Alloway KD, Mutic JJ, Hoover JE. Divergent corticostriatal projections from a single cortical
503 column in the somatosensory cortex of rats. *Brain Research*, 1998; 785: 341-6.
- 504 - Babb TL, Kupfer W. Phagocytic and metabolic reactions to chronically implanted metal
505 brain electrodes. *Experimental Neurology*, 1984; 86: 171-82.
- 506 - Borchers S, Himmelbach M, Logothetis N, Karnath HO. Direct electrical stimulation of
507 human cortex - the gold standard for mapping brain functions? *Nature Reviews Neuroscience*,
508 2012; 13: 63-70.
- 509 - Campbell A, Wu C. Chronically Implanted Intracranial Electrodes: Tissue Reaction and
510 Electrical Changes. *Micromachines*, 2018; 9.
- 511 - Cao F, Stan Leung L. Effect of atropine and PCPA on the behavioral modulation of paired-
512 pulse response in the hippocampal CA1 region. *Brain Research*, 1992; 576: 339-42.
- 513 - Cogan SF. Neural stimulation and recording electrodes. *Annu Rev Biomed Eng*, 2008; 10:
514 275-309.
- 515 - Conde V, Tomasevic L, Akopian I, Stanek K, Saturnino GB, Thielscher A, Bergmann TO,
516 Siebner HR. The non-transcranial TMS-evoked potential is an inherent source of ambiguity in
517 TMS-EEG studies. *Neuroimage*, 2019; 185: 300-12.
- 518 - David O, Bastin J, Chabardes S, Minotti L, Kahane P. Studying network mechanisms using
519 intracranial stimulation in epileptic patients. *Frontiers in Systems Neuroscience*, 2010; 4: 148.
- 520 - David O, Job AS, De Palma L, Hoffmann D, Minotti L, Kahane P. Probabilistic functional
521 tractography of the human cortex. *Neuroimage*, 2013; 80: 307-17.
- 522 - Dymond AM, Kaechele LE, Jurist JM, Crandall PH. Brain tissue reaction to some
523 chronically implanted metals. *J Neurosurg*, 1970; 33: 574-80.
- 524 - Enatsu R, Kubota Y, Kakisaka Y, Bulacio J, Piao Z, O'Connor T, Horning K, Mosher J,
525 Burgess RC, Bingaman W, Nair DR. Reorganization of posterior language area in temporal lobe
526 epilepsy: a cortico-cortical evoked potential study. *Epilepsy Res*, 2013; 103: 73-82.
- 527 - Entz L, Toth E, Keller CJ, Bickel S, Groppe DM, Fabo D, Kozak LR, Eross L, Ulbert I,
528 Mehta AD. Evoked effective connectivity of the human neocortex. *Human Brain Mapping*, 2014;
529 35: 5736-53.
- 530 - Eytan D, Brenner N, Marom S. Selective Adaptation in Networks of Cortical Neurons. *The*
531 *Journal of Neuroscience*, 2003; 23: 9349-56.
- 532 - Froc DJ, Chapman CA, Trepel C, Racine RJ. Long-Term Depression and Depotentiation
533 in the Sensorimotor Cortex of the Freely Moving Rat. *The Journal of Neuroscience*, 2000; 20: 438-
534 45.
- 535 - Geddes LA, Roeder R. Criteria for the selection of materials for implanted electrodes. *Ann*
536 *Biomed Eng*, 2003; 31: 879-90.
- 537 - Hartmann CJ, Hirschmann J, Vesper J, Wojtecki L, Butz M, Schnitzler A. Distinct cortical
538 responses evoked by electrical stimulation of the thalamic ventral intermediate nucleus and of the
539 subthalamic nucleus. *Neuroimage Clin*, 2018; 20: 1246-54.

- 540 - Heller U, Klingberg F. Evidence for cholinergic participation in frontal cortical potentials
541 evoked by single impulse stimulation in the locus coeruleus area of freely moving rats. *Biomed*
542 *Biochim Acta.*, 1989; 261-7.
- 543 - Hintiryan H, Foster NN, Bowman I, Bay M, Song MY, Gou L, Yamashita S, Bienkowski
544 MS, Zingg B, Zhu M, Yang XW, Shih JC, Toga AW, Dong HW. The mouse cortico-striatal
545 projectome. *Nat Neurosci*, 2016; 19: 1100-14.
- 546 - Keller CJ, Honey CJ, Megevand P, Entz L, Ulbert I, Mehta AD. Mapping human brain
547 networks with cortico-cortical evoked potentials. *Philosophical Transactions of the Royal Society*
548 *B: Biological Sciences*, 2014; 369.
- 549 - Kiebel SJ, Friston KJ. Statistical parametric mapping for event-related potentials (II): a
550 hierarchical temporal model. *Neuroimage*, 2004; 22: 503-20.
- 551 - Kubota Y, Enatsu R, Gonzalez-Martinez J, Bulacio J, Mosher J, Burgess RC, Nair DR. In
552 vivo human hippocampal cingulate connectivity: a corticocortical evoked potentials (CCEPs)
553 study. *Clinical Neurophysiology*, 2013; 124: 1547-56.
- 554 - Kumaravelu K, Oza CS, Behrend CE, Grill WM. Model-based deconstruction of cortical
555 evoked potentials generated by subthalamic nucleus deep brain stimulation. *J Neurophysiol*,
556 2018; 120: 662-80.
- 557 - Kunieda T, Yamao Y, Kikuchi T, Matsumoto R. New Approach for Exploring Cerebral
558 Functional Connectivity: Review of Cortico-cortical Evoked Potential. *Neurologia medico-*
559 *chirurgica*, 2015; 55: 374-82.
- 560 - Magill PJ, Sharott A, Bevan MD, Brown P, Bolam JP. Synchronous unit activity and local
561 field potentials evoked in the subthalamic nucleus by cortical stimulation. *Journal of*
562 *Neurophysiology*, 2004; 92: 700-14.
- 563 - Matsumoto R, Nair DR, LaPresto E, Najm I, Bingaman W, Shibasaki H, Luders HO.
564 Functional connectivity in the human language system: a cortico-cortical evoked potential study.
565 *Brain*, 2004; 127: 2316-30.
- 566 - Merrill DR, Bikson M, Jefferys JG. Electrical stimulation of excitable tissue: design of
567 efficacious and safe protocols. *J Neurosci Methods*, 2005; 141: 171-98.
- 568 - Oostenveld R, Fries P, Maris E, Schoffelen JM. FieldTrip: Open source software for
569 advanced analysis of MEG, EEG, and invasive electrophysiological data. *Comput Intell Neurosci*,
570 2011; 2011: 156869.
- 571 - Pidoux M, Mahon S, Deniau JM, Charpier S. Integration and propagation of
572 somatosensory responses in the corticostriatal pathway: an intracellular study in vivo. *J Physiol*,
573 2011; 589: 263-81.
- 574 - Prime D, Rowlands D, O'Keefe S, Dionisio S. Considerations in performing and analyzing
575 the responses of cortico-cortical evoked potentials in stereo-EEG. *Epilepsia*, 2018; 59: 16-26.
- 576 - Queiroz CM, Gorter JA, Lopes da Silva FH, Wadman WJ. Dynamics of evoked local field
577 potentials in the hippocampus of epileptic rats with spontaneous seizures. *J Neurophysiol*, 2009;
578 101: 1588-97.

579 - Rehnig HP, Brankack J, Klingberg F. Behaviour-dependent variability of potentials in the
580 somatosensory cortex evoked by stimulation of the trigeminal nuclei in freely moving rats. *Biomed*
581 *Biochim Acta.*, 1987; 46(4): 297-300.

582 - Robinson FR, Johnson MT. Histopathological studies of tissue reactions to various metals
583 implanted in cat brains. *AERONAUTICAL SYSTEMS DIV*, 1961.

584 - Rosenberg DS, Mauguiere F, Catenoix H, Faillenot I, Magnin M. Reciprocal
585 thalamocortical connectivity of the medial pulvinar: a depth stimulation and evoked potential study
586 in human brain. *Cereb Cortex*, 2009; 19: 1462-73.

587 - Rousche PJ, Pellinen DS, Pivin DP, Jr., Williams JC, Vetter RJ, Kipke DR. Flexible
588 polyimide-based intracortical electrode arrays with bioactive capability. *IEEE Trans Biomed Eng*,
589 2001; 48: 361-71.

590 - Stieglitz T, Meyer J-U. Implantable microsystems. Polyimide-based neuroprostheses for
591 interfacing nerves. *Medical device technology*, 1999; 10: 28-30.

592 - Trebault L, Deman P, Tuyisenge V, Jedynek M, Hugues E, Rudrauf D, Bhattacharjee M,
593 Tadel F, Chanteloup-Foret B, Saubat C, Reyes Mejia GC, Adam C, Nica A, Pail M, Dubeau F,
594 Rheims S, Trebuchon A, Wang H, Liu S, Blauwblomme T, Garces M, De Palma L, Valentin A,
595 Metsahonkala EL, Petrescu AM, Landre E, Szurhaj W, Hirsch E, Valton L, Rocamora R, Schulze-
596 Bonhage A, Mindruta I, Francione S, Maillard L, Taussig D, Kahane P, David O. Probabilistic
597 functional tractography of the human cortex revisited. *Neuroimage*, 2018; 181: 414-29.

598 - Trebault L, Rudrauf D, Job AS, Maliiia MD, Popa I, Barborica A, Minotti L, Mindruta I,
599 Kahane P, David O. Stimulation artifact correction method for estimation of early cortico-cortical
600 evoked potentials. *Journal of Neuroscience Methods*, 2016; 264: 94-102.

601 - Young JJ, Coulehan K, Fields MC, Yoo JY, Marcuse LV, Jette N, Panov F, Ghatan S,
602 Bender HA. Language mapping using electrocorticography versus stereoelectroencephalography:
603 A case series. *Epilepsy Behav*, 2018; 84: 148-51.

604 - Zosimovskii VA, Korshunov VA, Markevich VA. Conditions required for the appearance of
605 double responses in hippocampal field CA1 to application of single stimuli to Shaffer collaterals in
606 freely moving rats. *Neurosci Behav Physiol*, 2008; 38: 313-21.

607

608 **Figures and legends**

609 Figure 1: Electrodes' setup manufacturing. A. Take a pedestal and electrodes (four
610 stainless steel depth electrodes here). B. Bend them and cut them at the desired lengths
611 and angles to target brain areas you want. C. Check under a microscope the coating
612 integrity. D. Finally, glue all electrodes to the pedestal..... 5

613 Figure 2: Histological pictures after electrolytic lesion and Nissl staining for validate
614 electrodes localizations (in the somatosensory cortex on the left and in the dorso-lateral
615 striatum on the right)..... 10

616 Figure 3: A. Example of semi-automated movement artefact period removal. The blue
617 excluded part of the signal seems to be due to brief movement of the animal. B. Example
618 of artefact correction using a short interpolation combined with a longer exponential fit
619 (blue before correction and red after). This correction allows to free from the return-to-
620 zero time of the system and the sharp deflection of the stimulation artefact..... 11

621 Figure 4: Averaged signal to noise ratio curves for somatosensory cortex stimulation (on
622 the left, Nmin = 37 / Nmax = 39 recordings) and for the striatum (on the right, Nmin = 37 /
623 Nmax = 40 recordings) for each intensity of stimulation (error bars are standard error of
624 the mean values). 12

625 Figure 5: On the left (A), averaged correlation coefficient between individual trials and
626 CCEP for each intensity of stimulation (for stimulation in the somatosensory cortex in red
627 and in striatum in blue, with SEM superimposed) (Nmin = 2822 / Nmax = 3247 trials). On
628 the right (B), boxplot of correlation coefficients between 15-first and 15-last evoked
629 responses for each intensity of stimulation for all animals and all electrodes (N = 213
630 electrodes, with individual values superimposed)..... 13

631 Figure 6: Averaged evoked responses (Nmin = 17 and Nmax = 20 animals) and standard
632 errors of the mean (SEM) for each stimulated structure (striatum at the top and
633 somatosensory cortex at the bottom) and each recorded electrode. 14

634 Figure 7: Statistical analysis on time-frequency maps resulting from a first step of statistic
635 intra-animals consisting in a one-sample t-test across 2s-epochs of time-frequency maps
636 of each animal at the selected intensity of stimulation (number of 2s-epochs taken into

637 account: between 19 and 64 for the striatal stimulation and between 35 and 84 for the
 638 somatosensory cortex stimulation, data normality verified with Shapiro-Wilk test).
 639 Followed by a second step which is a two-sample t-test inter-animals allowing to identify
 640 the specific pattern of response obtained for each structure stimulated, for stimulation in
 641 striatum (A) and in somatosensory cortex (B). Surrounded areas are for a significance
 642 level of $p \leq 0.001$. Group sizes are noted above each statistical map ranging from 17 to
 643 20 animals. 15
 644 Figure 8: Statistical comparison of evoked responses between somatosensory stimulation
 645 and striatum stimulation. A and B for stimulations in right hemisphere, and C and D in the
 646 left one. A and C are recorded in the contralateral somatosensory cortex, and B and D in
 647 the contralateral striatum. Surrounded areas are significant values with $p \leq 0.001$ (two-
 648 sample t-test, $N_{min} = 17 / N_{max} = 20$ animals)..... 16
 649

650 **Highlights**

- 651 • New methodology using single pulse electrical stimulation in freely moving rats
- 652 • Responses to electrical stimulation were recorded in cortex and striatum
- 653 • Significant differences between cortical and subcortical responses
- 654 • Later components in striatal responses compared to cortical ones